

Effect of Carbonate and Chloride Ions on the Corrosion Susceptibility of Pipeline Steel Samples Artificially Aged

Perla Morales Gil^{1,*}, Manuel Palomar-Pardavé², María Guadalupe Montes de Oca-Yemha²,
María Teresa Ramírez-Silva³, Carlos Ángeles-Chávez¹, Mario Romero-Romo^{2,*}

¹ Instituto Mexicano del Petróleo, Laboratorio de Caracterización de Materiales Sintéticos y Naturales, Eje Central Lázaro Cárdenas 152, Ciudad de México, CDMX. CP 07730

² Universidad Autónoma Metropolitana-Azcapotzalco, Departamento de Materiales, Av. San Pablo 180 Col. Reynosa-Tamaulipas, Ciudad de México, CDMX. CP 02200

³ Universidad Autónoma Metropolitana-Iztapalapa, Departamento de Química, Av. San Rafael Atlixco #186, Col. Vicentina, Ciudad de México, CDMX. CP 09340.

*E-mail: moralesp@imp.mx (P.M.G) and mmrr@correo.azc.uam.mx (M.R.R.)

Received: 2 October 2017 / Accepted: 30 November 2017 / Published: 28 December 2017

This work deals with the corrosion behavior of pipeline steel samples (API 5L X52 and X70), artificially aged through heat treatment, in the presence of aqueous solutions containing either carbonate CO_3^{2-} , or chloride Cl^- anions, usually present during normal operating conditions. It was found from resistance to polarization measurements that Cl^- ions were more aggressive toward the materials tested than CO_3^{2-} . Furthermore, from thermodynamic predominance zone diagrams, PZD, and SEM-EDS characterization of the surfaces exposed to the corrosion environment, it is shown that Cl^- ions promoted formation of soluble Fe(II) chloro-complexes, which were the species produced during steel corrosion. These facilitated exposure of metal zones that had been first covered with corrosion products that formed under conditions of local chlorides-depletion, although now they had dissolved through the chloride interaction. This in fact eliminates the possibility of consolidating a passive layer. Conversely, when the CO_3^{2-} are present, dissolution of passivating products like insoluble Fe(II)- CO_3^{2-} complexes is less likely to occur, thus aiding to diminish the corrosion rate.

Keywords: artificial ageing; steel; corrosion; carbonates; chlorides; predominance zone diagrams

1. INTRODUCTION

The steel pipelines used for oil production are normally exposed to significant temperature variations that, even if they are low enough, they may result in ageing of the metallurgical microstructure. Other metal alloy systems illustrate well this phenomenon: it usually involves precipitation and growth of second-phase particles that have a positive impact on the mechanical

properties and time-dependent behavior of components built with alloys undergoing this phenomenon. However, the impact of ageing on the corrosion behavior has not been studied in depth. Pipelines transport oil, gas, refined products and other processing fluids, for great distances from production plants through diverse pumping, compressing, storing and distribution facilities. The steel products employed to fabricate pipelines must comply with API 5L (year 2000) standards. One limiting factor to useful pipeline life is corrosion, but when it interacts with mechanical factors, like residual stresses or strain cycles due to operating conditions, the result may lead to catastrophic failures at worst, with significant leakages induced, endangering thus the environment, urban areas and civil population. Therefore, the scale of the losses is rated against the gross national product, GNP. It is well known that as a consequence of significant service periods, pipelines reach diverse ageing stages [1,2], whereby, notable microstructural effects become apparent [3-5], for instance, formation of a variety of iron carbide-based nanoprecipitates that incorporate other elements added to sustain mechanical properties, participating in lesser proportions. Although, at first it may seem difficult to account for the activation forces involved, particularly at the low working temperature range proper of some systems, these are still capable of activating carbide-type nucleation and growth processes occurring typically in steels, that fall under the Ostwald ripening process. Consequently, it is elapsing time that controls slow growth of precipitates ranging in the nanometric to submicrometric scale. However, it has been stated [6], that ageing for 1 hour at 250 °C was considered equivalent to 2 year old-natural ageing. Therefore, the main effect on the materials microstructure, is the interaction amidst nanoprecipitates and numerous shifting dislocations, hindering their motion through the grain structure effectively. This constitutes a strengthening mechanism in the face of plastic deformation, which also brings about an increase in several mechanical properties. However, in this scenario ductility is adversely affected, reducing the yield to levels that delve gradually in the risk zone of failure, associated to increments or variations of the operating stresses. Heterogeneous concentration of stresses due to locking-dislocations mechanisms operating locally, seems a natural outcome once the carbide particles have reached sufficient size and density. This situation represents uncertainty, for residual stresses rise in the vicinities of grain boundaries where locking mechanisms and dislocation piles interact, then corrosion [6] may potentially be more active in connection with elastic deformation energy associated to local higher defect concentration at such localities. [8].

2. EXPERIMENTAL

Samples 0.95 cm² x 2.03 cm thick were cut from unused API 5L X52 and X70 pipelines with 36" OD. The supplier nominal composition is given in Table 1. Other samples slightly smaller were cut from the previous samples, 1 x 2 x 1 cm³ to conduct the artificial ageing experiments and SEM characterization, with a spark erosion machine to reduce the effect of cold work on the samples, to avoid unnecessary corrosion-promoting stored energy. Usual metallographic preparation was done down to polishing in alumina suspension with 0.25 µm particle size. Rinsing in absolute ethanol was followed by acetone ultrasonication for 5 minutes at room temperature.

Table 1. Nominal chemical composition of the steel samples.

| Sample | Composition, % wt | | | | | | |
|--------|-------------------|-------|-------|-------|-------|--------|--------|
| | Mn | Si | P | S | Al | Nb | |
| X52 | 1.06 | 0.26 | 0.019 | 0.003 | 0.039 | 0.041 | |
| X70 | 1.48 | 0.013 | 0.012 | 0.002 | 0.033 | 0.1 | |
| Sample | Composition, % wt | | | | | | |
| | Cu | Cr | Ni | V | Ti | N | Ca |
| X52 | 0.018 | 0.02 | 0.019 | 0.054 | 0.003 | | 0.0002 |
| X70 | 0.29 | 0.27 | 0.16 | 0.004 | 0.012 | 0.0027 | 0.0011 |

2.1 Artificial aging

Artificial ageing was carried out in a Lindberg furnace at 50 °C and 250 °C, during 100, 500 and 1000 h, respectively, under a flow of argon to prevent oxidation; thereafter the heat treated samples were air cooled.

2.2 Metallography

After artificial ageing heat treatment, the samples were mounted in transparent acrylic resin hardened at room temperature, to expose only one surface of the coupons. The ground blanks and heat treated samples microstructure was revealed through usual optical microscopy after 3% Nital acid attack.

2.3 Scanning electron microscopy

SEM characterization of the microstructures in the etched condition was done by means of secondary electron images from a Philips XL30 ESEM, also coupled with backscattered electron imaging (BSE) and energy dispersive spectrometer. The grain size measurements and quantitative optical microscopy were carried out using image and data processing through Image-Pro Plus V4.5 (Media CYBERNETICS Inc.), following ASTM E112-96 standard [9]. All SEM micrographs used for determination of the grain size were taken at 1000X magnification.

2.4 Electrochemical evaluation

A typical three-electrode cell served to carry out the electrochemical studies: the working electrodes were the steel samples prepared previously, while the reference electrode was a saturated calomel electrode, SCE, to which all potentials reported here should be referred to, and the counter electrode was a graphite bar with an exposed area larger by a factor of 2 to that of the working electrode (1 cm²). This geometric area, S, was used to calculate the current density as the ratio of the measured current and S. All working electrolytes were reagent grade NaCl and NaHCO₃ at: 0.1, 0.01,

and 0.001 M, respectively. Corrosion rates were measured through resistance to polarization scanning at 1 mV s^{-1} within the -20 to 20 mV respect to the open circuit potential, E_{oc} , using a EG&G PARC 273 potentiostat-galvanostat running the M352/252 data processing software that allowed communication, control and data acquisition through a PC.

Formation of a passive layer in 0.1 M NaHCO_3 media was evaluated by means of cyclic voltammetry at 50 mV s^{-1} using the M270 EChem data processing, at applied potentials more positive than E_{oc} . The construction of Predominance Zone Diagrams, PZD, was done following the well-known method established by Rojas-Hernández et al. [10-13]

3. RESULTS AND DISCUSSION

3.1 Influence of artificial ageing on steels corrosion susceptibility in the presence of chlorides

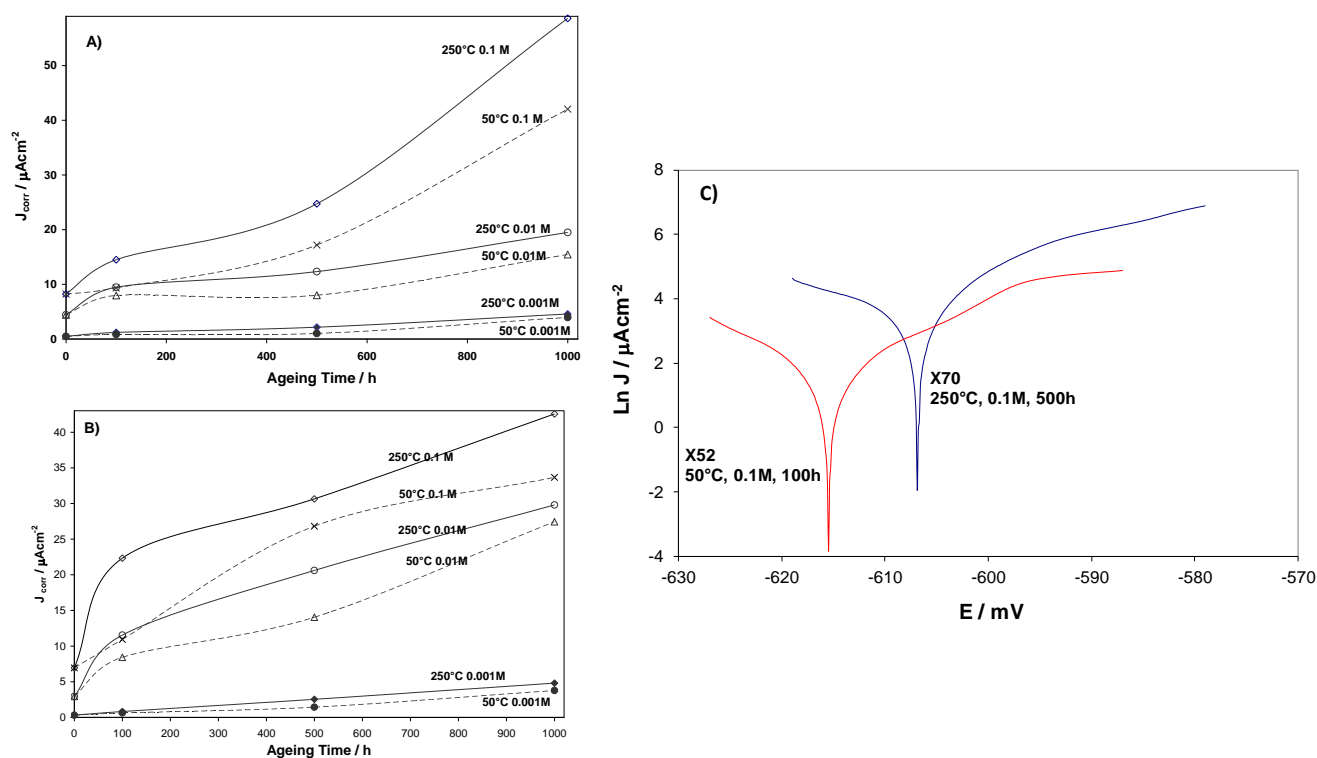


Figure 1. Variation of the corrosion current density as a function of the aging time recorded considering different chloride concentrations, and aging temperatures as indicated in the figures, and for A) X52 and B) X70. Corrosion measurements were performed at room temperature in static conditions. C) Some examples of Tafel plots used for J_{corr} estimation.

Figure 1 shows plots of the corrosion current density, J_{corr} , as a function of aging time for both pipeline steel samples API 5L X52, Fig A and X70, Fig. B along with typical Tafel plots from which J_{corr} was calculated, Fig. C. illustrating the effect of time, aging temperature and chloride concentrations on their corrosion rate. At constant chlorides concentration, the corrosion susceptibility

increased with increasing temperature and aging time, May *et al.* [14] studied the effect of thermal aging conditions on the corrosion properties of a duplex stainless steel and found that the corrosion resistance decreased steadily up to 5000 hours of aging. Also, increasing the chloride concentration increased the corrosion rate at constant aging time.

3.2 Predominance zone diagrams in the presence of chloride ions.

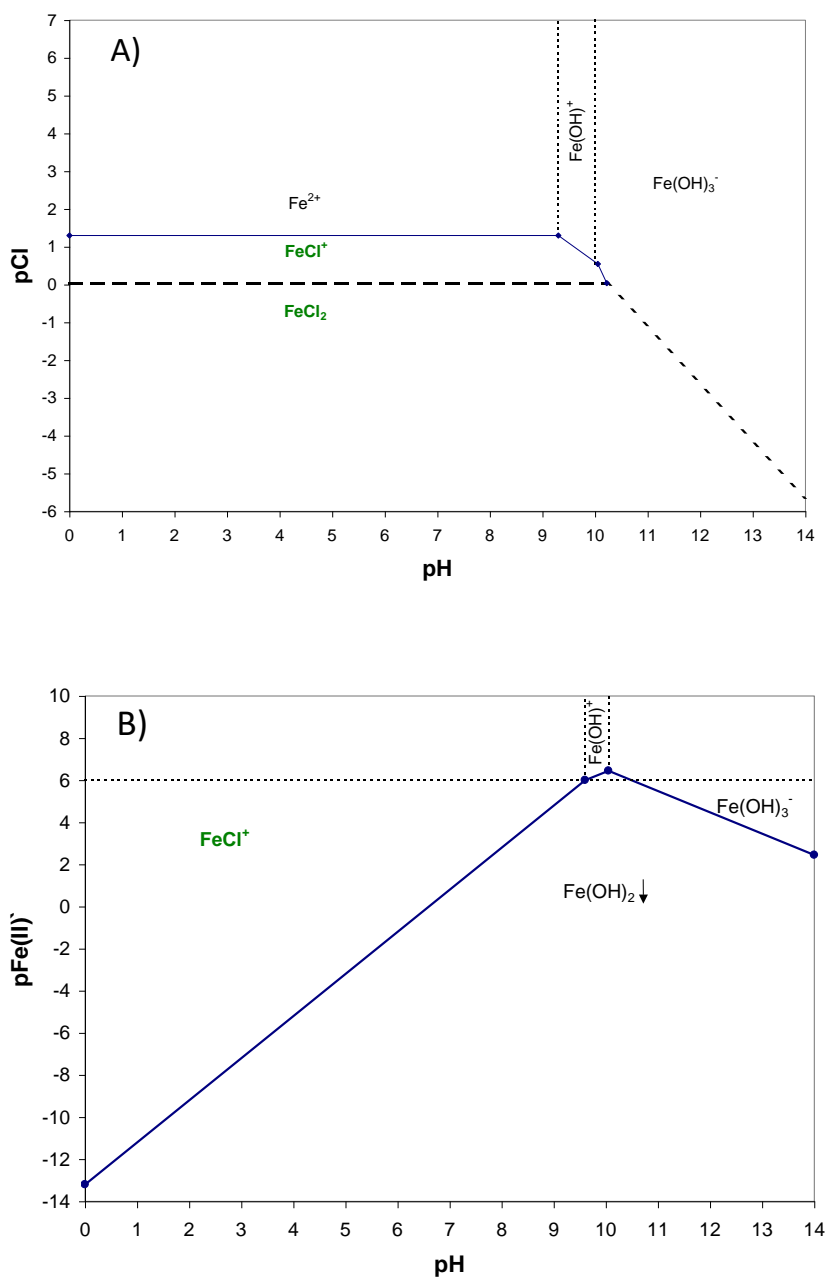


Figure 2. Predominance zone diagrams of the system: Fe(II)-Cl⁻-H₂O-H⁺ for A) Fe(II) soluble species and B) solubility (Fe(II) soluble and insoluble species) at 0.1 M NaCl.

The predominance zone diagrams, PZD of the system: Fe(II)-H₂O-H⁺-Cl⁻ is shown in Figure 2a, considering solely soluble species. It is possible to note that for pCl < 0.9, the formation of Fe(II) chloro-complex, like FeCl⁺ is thermodynamically favored. The diagram shown in Figure 2A indicates that the presence of the Fe(II) chloro-complex must be considered whenever the Cl⁻ concentration is 0.1 M, which increases the overall corrosion rate. Furthermore, Figure 2B depicts the solubility of Fe(II) insoluble species at a 0.1 M chloride concentration and shows that at pH 6.8, namely the pH of the NaCl solution, FeCl⁺ is the predominant species in. This underlines the ample predominance range of the chloro-complex and that in order to be able to form a (Fe(OH)₂) precipitate, quite a high Fe(II) concentration would be needed in solution, pFe(II) < -1.2 under the present working conditions. To supply such an amount of Fe(II) the rate of dissolution must be sufficiently high, which explains the reasons underlying the increased corrosion rate in the presence of chlorides.

Figure 3 shows the Pourbaix-type diagram produced for the system at hand: Figure 3A shows the diagram depicting the species and their interactions in the Fe(0)-Fe(II)-Fe(III)-H₂O-Cl⁻ system, considering a 10⁻⁶ M Fe(II) concentration and a 0.1 M NaCl concentration. It can be observed that predominance of the FeCl⁺ is dependent on potential and pH. For the sake of argument, this sort of diagram can be divided in three main zones; Figure 3B shows that the first zone is ascribed to immunity, where the potential is negative enough and the pH acid enough to warrant the thermodynamic stability of the metal state, so there is no dissolution of the steel substrate in the presence of the electrolyte. The second region is called passivity zone, which is where corrosion rate is so moderate that, for practical purposes, the dissolution is considered a sluggish process, in fact practically negligible, thought to be due to the presence a layer composed of insoluble corrosion products, such as oxides or hydroxides, as shown in Figure 3A, formed during the initial exposure instants, attached to the surface of the substrate, effectively precluding further contact between metal and electrolyte. The physicochemical characteristics of this layer, such as its inherent capability to allow mass transport through its lattice, will then exert control on the overall rate of corrosion to form other species such as Fe(OH)₃, as can be observed in Figure 3A. Thus, the reason to call it passive state may be easily surmised.

Finally, the region associated to electrochemical activity, is also termed corrosion zone; the name leads to gather that potential and pH make FeCl⁺ and Fe³⁺ the stable species in solution. Therefore, line A in Figure 3B represents the hydrogen redox process, such that at fixed pH, when the systems' potential has a value below this broken line (more negative value), the stable species would be gaseous hydrogen evolving, indeed from the surface of the working electrode. The present study was carried out with the aim of showing that the presence of chloride ions alters the position of the Fe corrosion-passivity line. Therefore, the behavior observed on the aged samples, proved that greater corrosion susceptibility prevails in the presence of 0.1 M NaCl than for the other two concentrations, namely 0.01 M and 0.001 M. Further, it was found that at pH 6 the system is located within an active zone, whereby there was a rapid dissolving attack likely due to a relatively high chlorides concentration over the areas exposed.

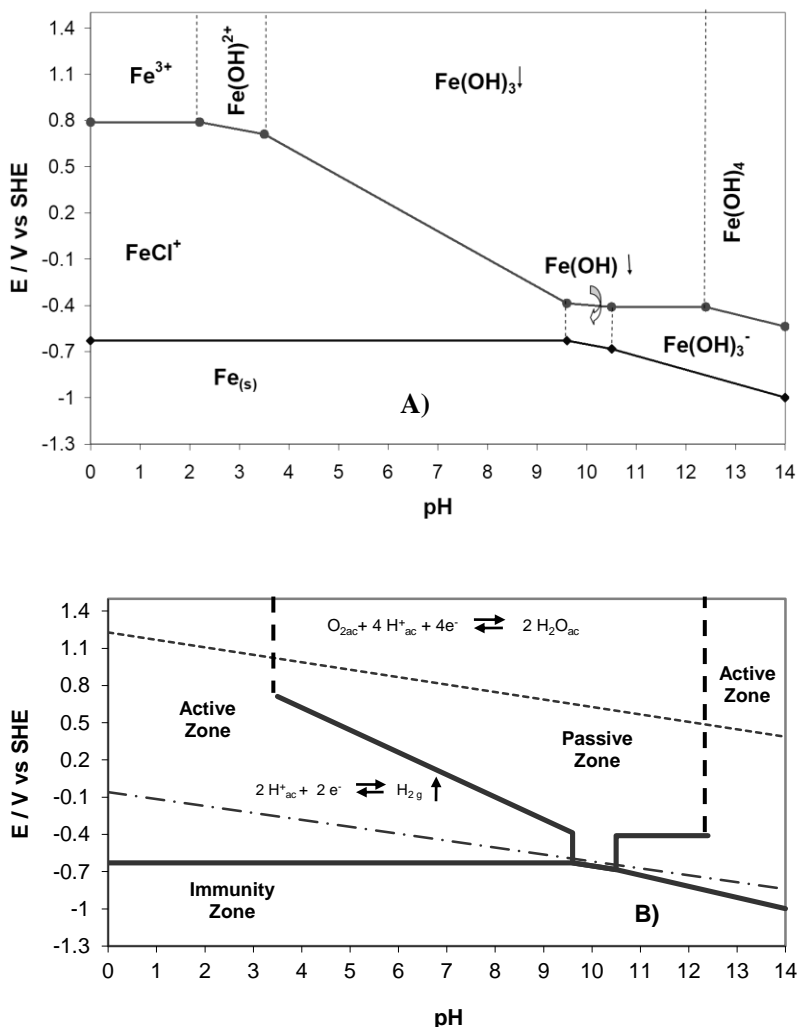


Figure 3. Pourbaix type diagrams of the system A) Fe(0)-Fe(II)-Fe(III)-H₂O-Cl' and B) distribution of electrochemical activity zones relative to a 0.1 M NaCl concentration, considering a 10⁻⁶ M iron concentration.

This explains feasibly the experimental observation that corrosion rates increase with increasing chloride concentration in the electrolyte, because of formation of a soluble chloro-Fe(II) complex, the stability of which determines the corrosion velocity, or that the surface is maintained in an active state within the relatively ample stability range for the chloride-containing iron species in solution.

3.3 Effect of steel aging on the corrosion susceptibility in the presence of carbonates

Figure 4 shows a plot of the corrosion susceptibility of the API 5L X52 steel samples as a function of artificial aging time at two temperatures immersed in the NaHCO₃ solutions with different concentrations. As shown, when the [NaHCO₃] = 0.1 M, the corrosion rate was smaller compared to the other two working concentrations, namely, 0.01 M and 0.001 M. This suggests that a passive

surface layer is exerting control on the metal substrate wastage rate. The effect of ageing can be noted for that CO_3^{2-} concentration of 0.1 M.

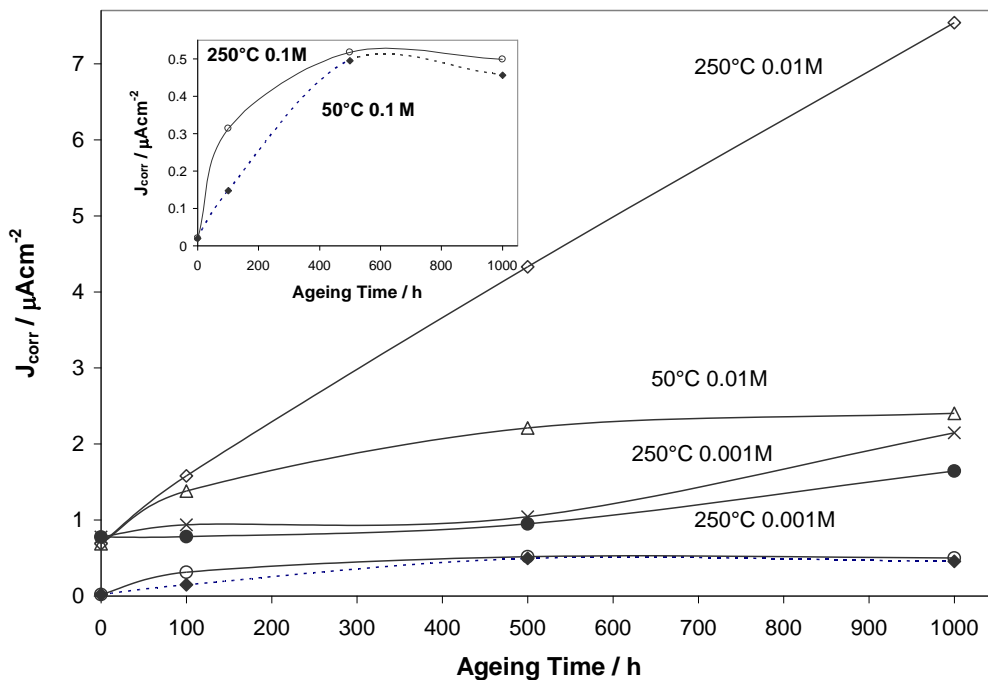


Figure 4. Corrosion rate variation of the X52 samples heat treated at 50 °C and 250 °C as a function of aging time, immersed in NaHCO_3 solutions having different concentrations at ambient temperature in static conditions.

It is relevant to compare the corrosion rate increment of the sample aged at 250 °C for 1000 h immersed in a 0.01 M CO_3^{2-} solution with that of the sample aged for the same period at the lower temperature of 50 °C. Figure 4 indicates that the apparent increment was $5.1 \mu\text{A cm}^{-2}$, which turned out to be the greatest increment observed for this series of samples. The comparison emphasizes that, at a constant carbonate concentration, when both steel samples X52 and X70 were artificially aged at the accelerated rate imparted by heat treatment at 250 °C, they were more susceptible to corrosion as a function of increasing ageing time.

3.3.1 Passivation of the steel API 5L X52

Figure 5 shows a typical comparison of the current densities of the X52 steel samples aged and tested in the carbonate-containing solutions. The results shown in Figure, obtained after heat treatment at 250 °C for 500 h, can be considered typical compared to the results from longer aging times. However, it is relevant to highlight these results because they indicate that the sample immersed in the 0.01 M carbonate solution appeared to corrode at a faster rate; this behavior was revealed through cyclic voltammetry, because the sample did not exhibit a passivating potential. However, at the higher 0.1 M concentration the plot suggested the presence of a passivating product on the sample surface. It is important to stress that Sadeghi Meresht et al. [15] have shown that API X65 steel pipeline, without being subjected to any artificial aging process, immersed in a 2M carbonate/ 1M bicarbonate solution

depicts a corrosion current of $3.7 \mu\text{Acm}^{-2}$, see Table 1 in [15]. This value is lower than that found in this work in the absence of carbonates which further support the outcome about passivation of the steel in the presence of carbonate ions finding in this work.

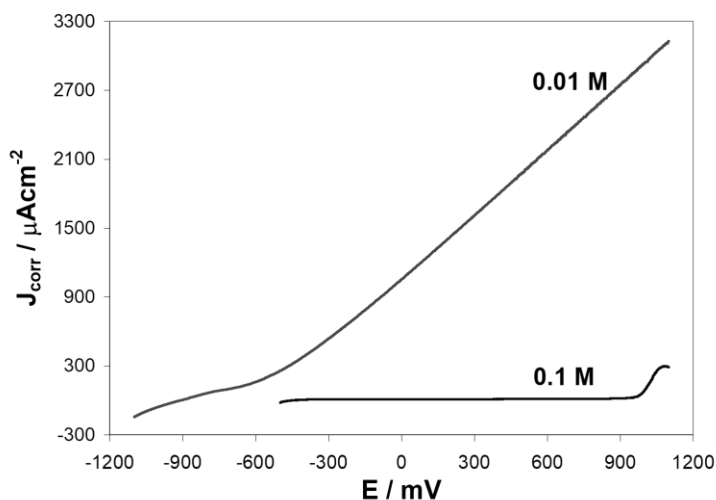


Figure 5. Electrochemical behavior of the X52 samples artificially aged at 250 °C for: 500 h immersed in NaHCO_3 aqueous with two different concentrations indicated in the figure.

Figure 6 (a) shows the backscattered electron image of the surface topography obtained with the SEM at 50 X, on the X52 sample artificially aged at 250 °C, after cyclic voltammetry immersed in the carbonate solution that reveals formation of a crinkle surface layer that delineates the underlying grain boundary steel structure. There is a generalized lack of contrast diversity in the image, indicating that it is mostly formed by iron. Figure 6 (b) is the qualitative chemical analysis from energy dispersive spectrometry, which displays the iron, sodium and oxygen main peaks and a couple of small peaks belonging to carbon and sulfur.

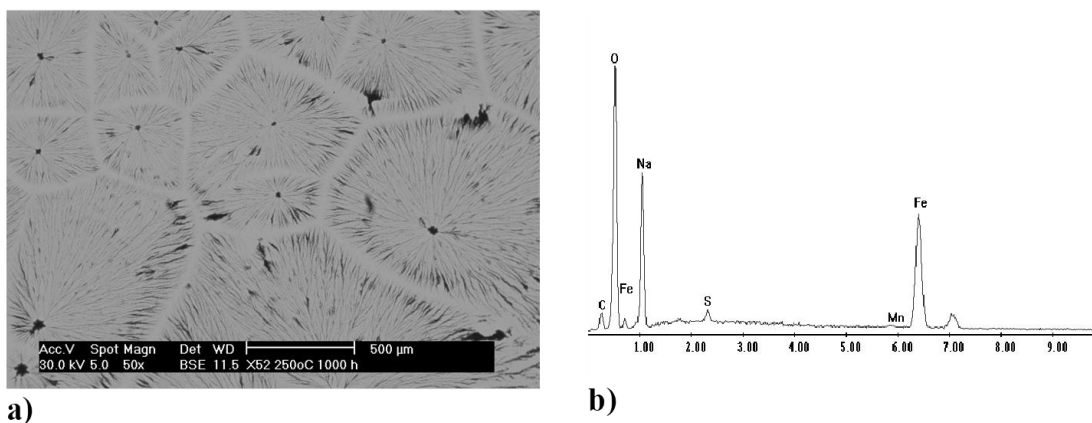


Figure 6. a) BSE image of an X52 sample aged at 250 °C, immersed in the 0.01 M NaHCO_3 solution that reveals the presence of a striated corrosion product surface layer, and **b)** EDS spectrum denoting mainly the presence of O, Na, Fe, with C and S displaying the smallest peaks.

The morphology of the corrosion product was examined with the aim to establish a means of comparison regarding the effect of carbonate concentration on the morphology of the corrosion

resulting product, after corrosion testing the X52 sample under the same ageing time at one particular temperature. Figure 7 (a) corresponds to the sample aged for 1000 h at the 0.01 M carbonate concentration, exhibiting an almost featureless surface layer that may be associated to its thin nature; also, this Figure shows in the backscattered electron micrograph, the presence of a few stains of varied sizes, over the surface area selected. Without an appreciable relief these marks seem to be fissured, probably due to local interfacial stresses.

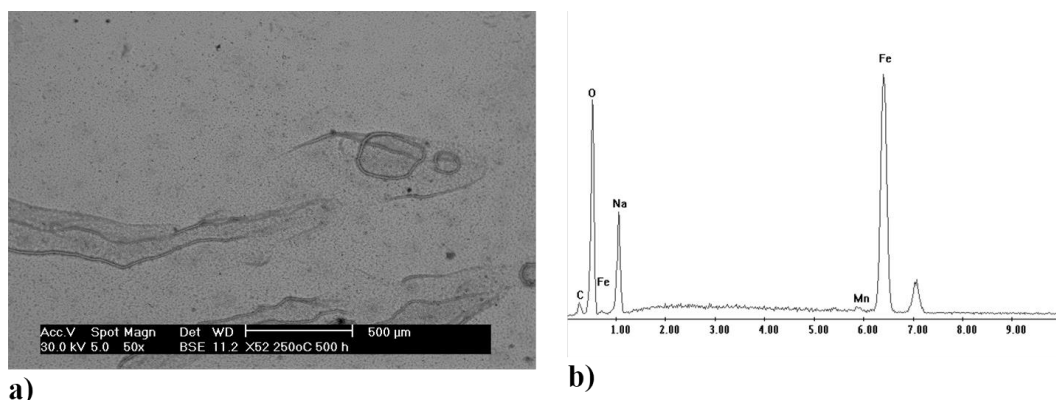


Figure 7. a) BSE image of an X52 sample aged at 50 °C, immersed in the 0.01 M NaHCO_3 for 1000 h solution that reveals the presence of an apparently more uniform surface corrosion product, devoid of particular topographical features, and b) EDS spectrum from one of the elongated darker surface mark where the Fe peak was more intense. The O and Na peaks were second and third in relative intensity.

The EDS elemental analysis shown in Figure 7 (b), recorded over the elongated dark marks, revealed mostly the presence of Fe, then O, Na and small peak of C, forming the surface corrosion product that displayed a plain morphology, proper of a thin surface deposit layer. This is in contrast with the corrosion products layer formed on the higher temperature heat treated-X52 sample, exposed also to the 0.01 M carbonate solution, that formed a thicker layer covering the metal substrate. At plain view it displayed a yellow color.

It is pertinent to add that for the X70 samples, the cyclic voltammetry testing in both carbonate concentrations, namely 0.1 and 0.01M, and the morphologies that resulted were indeed similar to those already discussed for the X52 steel.

3.3.2 Predominance zone diagrams for carbonate species

In order to build a viable basis to explain the observed corrosion rates of the aged samples that were exposed to different carbonate's concentration, it was thought just as appropriate as in the previous case, to build diagrams for the distribution of species in solution different pCO_3 values as a function of pH in the $\text{Fe(II)}-\text{H}_2\text{O}-\text{CO}_3$ system. Figure 8 (a) shows the diagram developed where the a, b and c represent the graph locus to plot the working carbonate concentrations, namely, 0.1 M, 0.01 M and 0.001 M, respectively. From a detailed analysis of each pCO_3 line, it becomes apparent that different soluble chemical species exist for each carbonate concentration, be it as hydroxo-complexes

or as iron carbonates. Further, a diagram of insoluble species was developed for carbonate species and for iron hydroxide that is shown in Figure 8 (b). As before, the lines a, b and c represent the location of the working carbonate solutions employed. Given that the pH values of the carbonate working solutions, namely 8.63, 8.66 and 8.4, all fall in the basic range, the possibility of competition between iron carbonate and iron hydroxide species is not likely. Thus, if an imaginary line were traced in the solubility diagram, dependent on pH and solution concentration, it becomes clear that under the working conditions, only the precipitation of iron carbonate will occur.

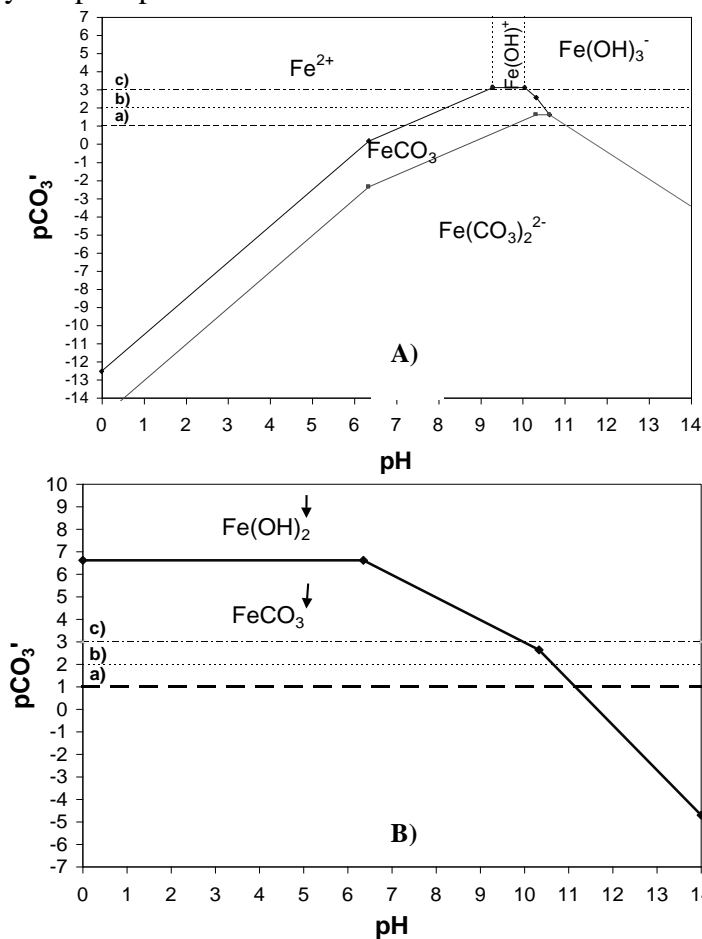


Figure 8. Predominance zones species diagrams for the formation of: A) soluble and insoluble species. B) Interconversion of precipitates in the system: $Fe(II)-H_2O-CO_3'$. The lines a, b and c indicate the working concentrations, 0.1, 0.01 y 0.001 M, respectively.

In order to gather further information on the soluble and insoluble species formed when exposing the steel to varying CO_3^{2-} concentrations, the following system was studied $Fe'-H_2O-CO_3'$ to enable plotting $pFe(II)$ as a function of pH at different carbonates concentration. Therefore, Figure 9 shows the diagrams containing the distribution of the species in the system proposed at different $pFe(II)$ values. It becomes clearly observable that drawing a line at pH 8.63 to reach an $Fe(II) 10^{-6}$ M concentration, it falls nearly half way through the predominance zone of the $FeCO_3$ solid species. Therefore, it is possible to say that the passive layer formed under this condition corresponds to iron carbonate, $FeCO_3$. Figure 9 (b) corresponds to a 0.01 M carbonate concentration, where it can be

appreciated that the dot located at the coordinates given by pH 8.66, representing the solution pH, and the value 6 that corresponds to a low iron Fe(II) concentration, falls within the insoluble FeCO_3 predominance zone. Further, based on this diagram it becomes possible to say that the precipitate formed at the 0.01 M concentration is FeCO_3 , although it tends to dissolve, thereby making it incapable of forming a protective layer, this being a feature that is associated with observed increments of the corrosion rate.

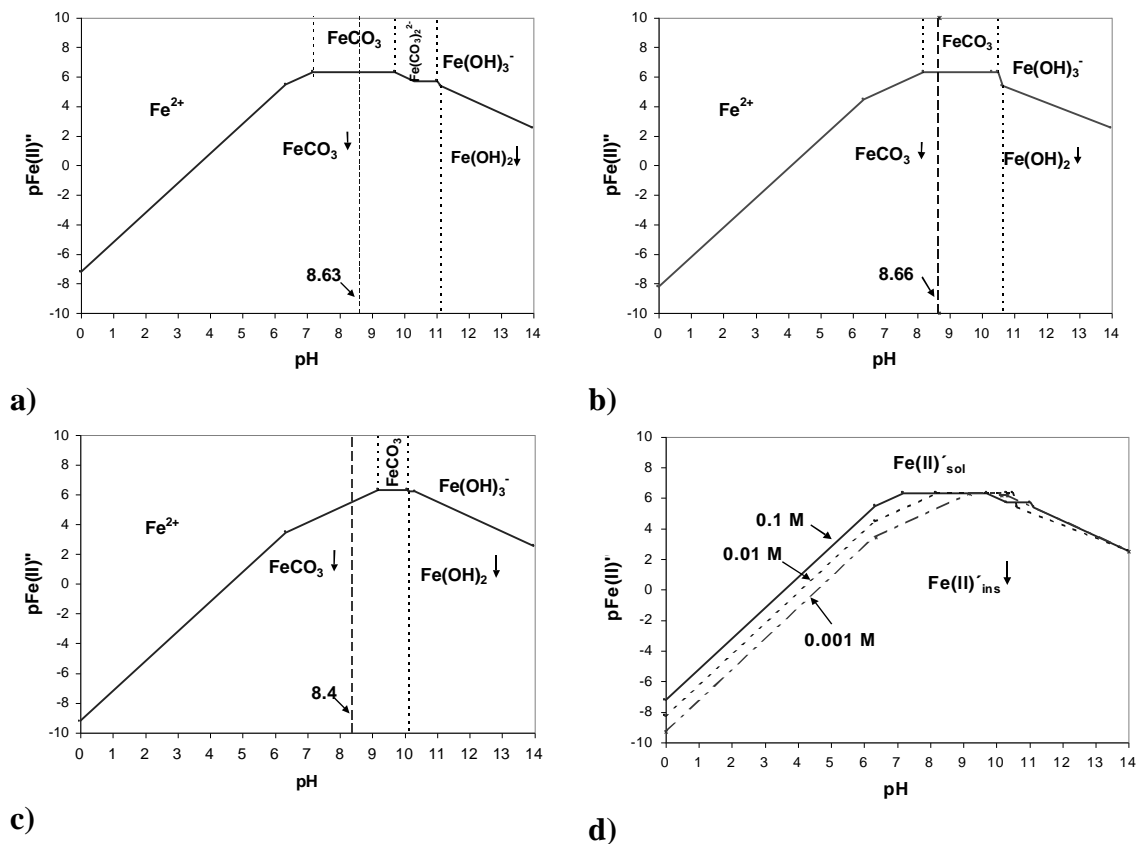


Figure 9. Soluble and insoluble carbonate species predominance zones diagrams as a function of pFe(II) and pH in the system $\text{Fe(II)}^{2+}\text{-H}_2\text{O-CO}_3^{2-}$, estimated for three different carbonate concentrations: a) 0.1 M, b) 0.01 M and c) 0.001 M. d) Comparison of the diagrams for the distribution of species at the three concentrations.

Figure 9 (c) was obtained at 0.001 M carbonates concentration; it can be observed that at the solution $\text{pH } 8.4$ and at 10^{-6} M Fe(II) , there is no formation of solid carbonate products constituting a passivating layer, thus the likely happening is the dissolution of the steel substrate to form Fe^{2+} proceeds as depicted in the diagram. Therefore, it would be expected to have a high corrosion rate in the said 0.001 M carbonate solution. Actually, this is not what happens mainly because the carbonate concentration is low enough to facilitate formation of the iron-based carbonate complex, apart from the fact that a 10^{-4} M Fe concentration would be required for such a purpose. Lastly, when the three solubility lines of the corresponding carbonates concentrations are superimposed, it can be observed that as the concentration decreases the Fe(II) solubility increases, as shown by Figure 9 (d). These findings also apply to both X52 and X70 steels, similarly to the voltammetry results. It is relevant to

add that other chemical species might exist in these diagrams, though as their constants have not been reported, it is not viable to consider them part of this theoretical analysis.

3.4 Effect of the aged steels microstructure

The results concerning the measurements of the grain size and pearlite percent will be presented below, as two metallurgical factors that may have an effect on the corrosion behavior of the aged steels. Figure 10 (a) shows that the corrosion rate increased with increasing grain size, however, these increments seem affected by increasing chloride concentration, as stated previously.

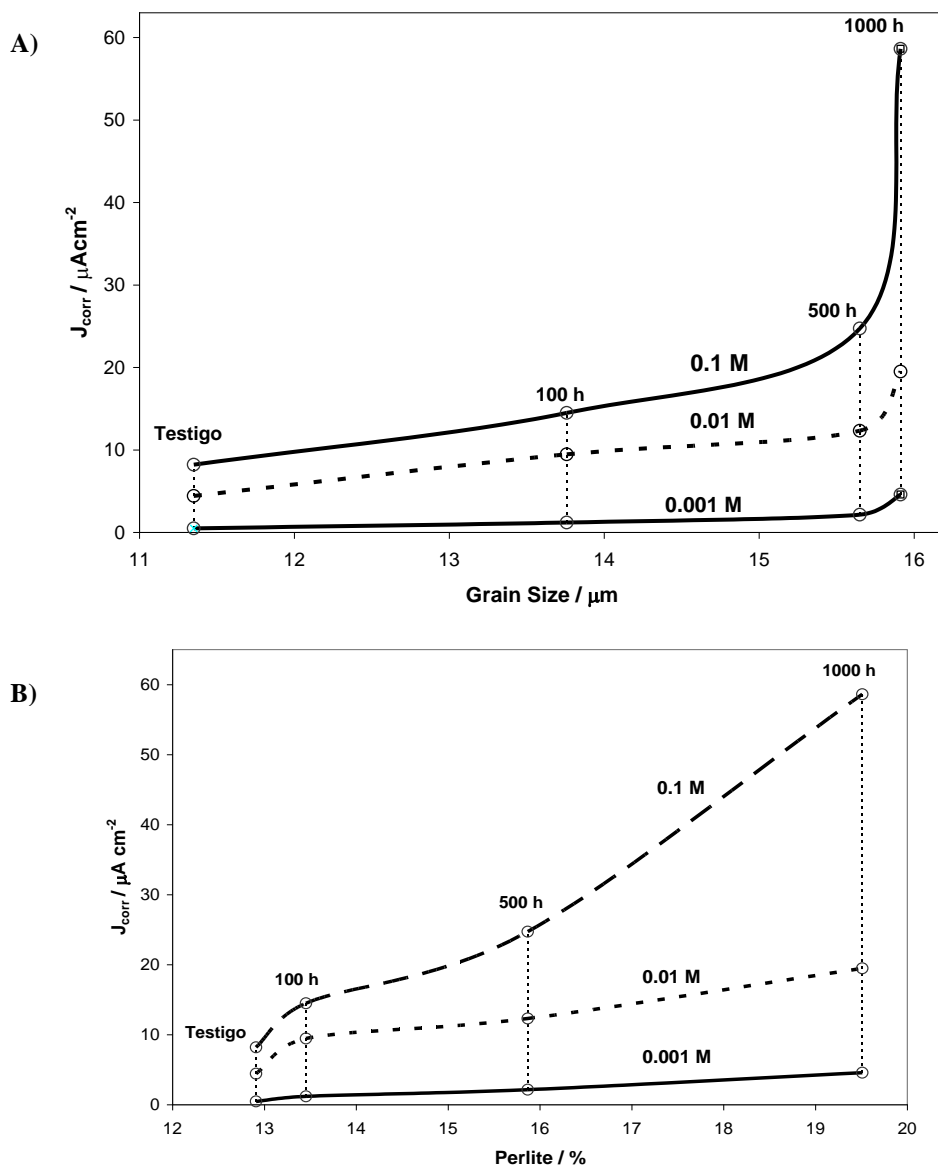


Figure 10. Comparison of corrosion current densities as a function of: A) grain size and B) of the pearlite content in the X52 steel sample aged at 250 °C for various times, immersed in electrolyte solutions with different chloride contents.

It is relevant to consider that the grain size increase is ascribed to steels grain coalescence coupled with a relatively marginal size increase of the pearlite colonies. Regarding the latter, the corrosion rate increment was also observed to rise with percent content of pearlite colonies, as suggested by Figure 10 (b). This can be attributed to formation of galvanic microcells between the pearlite constituents, namely the more active member, α -iron or ferrite that contains very low carbon, and the nobler member, iron carbide Fe_3C , both of which would couple electrochemically before the electrolyte, thus contributing to increase the rate, and this perhaps is more pronounced at the ferritic grain boundaries which are inherently electrochemically active. It would seem plausible therefore, to explain the increased corrosion rate as a function of an increased number of pearlite colonies, or galvanic microcells area. It is important to say that, the X70 samples showed a similar tendency concerning the increased corrosion rate related to pearlite size, also in the presence of carbonates.

4. CONCLUSIONS

Artificial aging was induced in API 5L 52 and X70 pipeline steel samples through low temperature heat treatment to exert microstructural modifications on the grain size and pearlite contents: both aspects increased with increasing heat treatment temperature and ageing time. The increased grain size was due to coalescence and the changes in pearlite contents to redistribution of carbon.

The greater susceptibility to corrosion in the presence of chlorides or carbonates was associated with the pearlite morphology changes observed, due to formation of a greater number of galvanic pairs throughout the exposed surface.

The chloride-containing solutions were found to promote greater corrosion rates than those containing carbonates. From the thermodynamic analysis performed, the resulting predominance zones diagram, PZD, together with elemental analysis characterization through SEM+EDS of the surface and corrosion products, made it clear that the presence of Cl^- in solution gives rise to formation of soluble Fe(II) chloro-complexes as reaction products directly responsible of the dissolution rate of the steel. Under the working concentrations imposed, there were no possibilities to induce formation of insoluble products capable of blocking surface active sites through formation of a passivating film on the substrate surface, hence to decrease effectively the rate of corrosion. On this same respect, when carbonates are present in solution, the mechanism is different, because it is affected by the presence of a passivating FeCO_3 film depending on the concentration, which exerts control on the corrosion rate of the materials.

Steel X52 samples exhibited greater susceptibility to corrosion in the presence of chlorides as compared to X70 steel samples, because the pearlitic colonies appeared larger as the grains size also was bigger.

ACKNOWLEDGEMENTS

M.R.R. and M.P.P. would like to thank CONACYT for project 22610714. M.R.R., M.T.R.S., M.G.M.Y. and M.P.P. gratefully acknowledge the SNI for the distinction of their membership and the stipend received.

References

1. J.Q. Wang, A. Atrens. *Corros. Sci.*, 45 (2003) 2199.
2. M.K. Miller, J. Bentley. *Mat. Sci. Technol.* 6, (1990) 285.
3. S.H. Avner. *Introduction to Physical Metallurgy*, McGraw-Hill (1988)
4. R.E. Smallman, R.H.W Ngan, *Physical Metallurgy and Advanced Materials*, Butterworths-Heinemann, Seventh edition (2007).
5. Y. Krasowsky, Y. Meshkov, V.M. Torop, *Int. J. Pressure Vessels Piping*, 81 (2004) 337.
6. A. Vargas-Arista, Albitier, C. ÁngelesChávez and J. M. Hallen, *Metall Mater Trans A*, vol. 37A (2006) 2683.
7. M. Corrales-Luna, O. Olivares-Xometl, N.V. Likhanova, R.E. Hernández Ramírez, I.V. Lijanova, P. Arellanes-Lozada, E. Arce Estrada. *Int. J. Electrochem. Sci.*, 12 (2017) 6729.
8. J.L. Kennedy. *Oil and Gas Pipeline, Fundamentals*, 2nd. ed. Ed. PennWell Books, ISBN 0-87814-390-4, Tulsa, Oklahoma, (1993) chapter 3.
9. ASTM E112-96. (1996) Standard Test Methods for Determining Average Grain Size.
10. A. Rojas-Hernández, M.T. Ramirez, J.G. Ibáñez, I. Gonzalez. *J. Electrochem. Soc.*, 138 (1991) 365.
11. A. Rojas-Hernández, M.T. Ramírez, J.G. Ibáñez, I. González. *Anal. Chim. Acta*, 246(2), (1991) 435.
12. A. Rojas-Hernández, M.T. Ramírez, I. González, J.G. Ibáñez. *Anal. Chim. Acta*, 259(1), (1992) 95.
13. A. Rojas-Hernández, M. T. Ramírez, I. González. *Anal. Chim. Acta*, 278(2) (1993) 335.
14. J.E. May, C.A. Caldas de Souza, P.A. de Paula Nascente, P. Soares, C.M. Lepienski, S. E. Kuri. *Materials Research*. 13 (2010) 431.
15. E. Sadeghi Meresht, T. Shahrabi Farahani, J. Neshati. *Corros. Sci.*, 54 (2012) 36.